A Method for Connecting Dissimilar Finite Element Meshes in Three Dimensions [1]

C. R. Dohrmann[2]
S. W. Key[3]
M. W. Heinstein[3]

Abstract. A method is presented for connecting dissimilar finite element meshes in three dimensions. The method combines the concept of master and slave surfaces with the uniform strain approach for finite elements. By modifying the boundaries of elements on the slave surface, corrections are made to element formulations such that first-order patch tests are passed. The method can be used to connect meshes which use different element types. In addition, master and slave surfaces can be designated independently of relative mesh resolutions. Example problems in three-dimensional linear elasticity are presented.

Key Words. Finite elements, connected meshes, uniform strain, contact.

---

[1]Sandia is a multiprogram laboratory operated by Sandia Corporation, a Lockheed Martin Company, for the United States Department of Energy under Contract DE-AL04-94AL8500.

[2]Structural Dynamics Department, Sandia National Laboratories, MS 0439, Albuquerque, New Mexico 87185-0439, email: crdohrm@sandia.gov, phone: (505) 844-8058, fax: (505) 844-9297.

[3]Engineering and Manufacturing Mechanics Department, Sandia National Laboratories, MS 0443, Albuquerque, New Mexico 87185-0443.

DISCLAIMER

DISCLAIMER

1. Introduction

In order to perform a finite element analysis, one may be required to connect two meshes at a shared boundary. Such requirements are common when assembling system models from separate subsystem models. One approach to connecting the meshes requires that both meshes have the same number of nodes, the same nodal coordinates, and the same interpolation functions at the shared boundary. If these requirements are met, then the two meshes can be connected simply by equating the degrees of freedom of corresponding nodes at the shared boundary. As might be expected, connecting meshes in this manner often requires a significant amount of time and effort in mesh generation.

An alternative to such an approach is to use the concept of "tied contact" to connect the meshes. With this concept, one of the connecting mesh surfaces is designated as the master surface and the other as the slave surface. For problems in solid mechanics, the meshes are connected by constraining nodes on the slave surface to specific points on the master surface at all times. Although this approach is appealing because of its simplicity, overlaps and gaps may develop between the two meshes either because of non-planar initial geometry or non-uniform displacements. For example, a node on the master surface may either penetrate or pull away from the slave surface during deformation even though the slave node constraints are all satisfied. As a result, displacement continuity may not hold at all locations on the master-slave interface.

Several methods currently exist for connecting finite elements or meshes of elements. Mesh grading approaches allow two or more finer elements to abut the edge of a neighboring coarser element [1]. Although such approaches generate conforming element boundaries,

they are not applicable to the general problem of connecting two dissimilar meshes. Other methods [2-3] for connecting meshes based on constraint equations or Lagrange multiplier approaches are applicable to a much broader class of problems, but they generally do not ensure that mesh boundaries conform during deformation. Finite element approaches developed specifically for contact problems can also be used to connect meshes. These [4] include: (i) Lagrange multiplier methods; (ii) penalty methods; and (iii) mixed methods. Many of these methods are based in part on the master-slave concept.

Regardless of the method used to connect two meshes, it is important to address the issues related to continuity at the mesh boundaries. One such issue is the first-order patch test [5]. In general, meshes that are connected using existing methods based on constraint equations or penalty functions alone fail the patch test. A general method for connecting finite element meshes in two dimensions that passes the patch test was developed recently by the authors [6]. This study investigates an extension of that method to three dimensions. The basic idea is to redefine the boundaries of elements on the slave surface to achieve a conforming connection with the master surface. The same idea was used recently at the element level to obtain a conforming transition between hexahedral and tetrahedral elements [7].

The present method combines the master-slave concept with the uniform strain approach for finite elements [8]. As with the standard master-slave approach, nodes on the slave surface are constrained to the master surface. In addition, the boundaries and formulations of elements on the slave surface are modified to ensure that first-order patch tests are passed. Consequently, results obtained using the method converge with mesh refinement.

A useful feature of the method is the freedom to designate the master and slave surfaces

independently of the resolutions of the two meshes. Standard practice commonly requires the surface designated as the *master* to have fewer numbers of nodes than the slave surface. The present method allows one to specify either of the mesh boundaries as master while still satisfying the patch test. It is shown in Section 3 that improved accuracy can be achieved in certain instances by allowing the master surface to have the greater number of nodes. Thus, there may be a preferred choice for the master surface in certain cases. Methods of mesh refinement based on adaptive subdivision of existing elements may also benefit from the method. For example, kinematic constraints on improper nodes could be removed while preserving displacement continuity between adjacent elements.

Details of the method are presented in the following section. The presentation includes a discussion of the uniform strain approach and the geometric concepts upon which the method is based. Example problems in three-dimensional linear elasticity are presented in Section 3. These examples highlight the various capabilities of the method. Comparisons made with the standard master-slave approach demonstrate the superior performance of the method.

2. Formulation

Consider a generic finite element in three dimensions with nodal coordinates x_{iI} and nodal displacements u_{iI} for $i = 1, 2, 3$ and $I = 1, \ldots, N$. The spatial coordinates and displacements of a point in the global coordinate direction $\mathbf{e}_i$ are denoted by x_i and u_i, respectively. For isoparametric elements, the same interpolation functions are used for the coordinates and displacements. That is,

$$x_i = x_{iI}\phi_I(\eta_1, \eta_2, \eta_3) \tag{1}$$

$$u_i = u_{iI}\phi_I(\eta_1, \eta_2, \eta_3) \tag{2}$$

where ϕ_I is the shape function of node I and (η_1,η_2,η_3) are isoparametric coordinates. A summation over all possible values of repeated indices in Eqs. (1-2) and elsewhere is implied unless noted otherwise.

The Jacobian determinant J of the element is defined as

$$J = \det \begin{bmatrix} \partial x_1/\partial\eta_1 & \partial x_2/\partial\eta_1 & \partial x_3/\partial\eta_1 \\ \partial x_1/\partial\eta_2 & \partial x_2/\partial\eta_2 & \partial x_3/\partial\eta_2 \\ \partial x_1/\partial\eta_3 & \partial x_2/\partial\eta_3 & \partial x_3/\partial\eta_3 \end{bmatrix} \tag{3}$$

The volume V of the element can be expressed in terms of J by

$$V = \int_{V_\eta} J dV \tag{4}$$

where V_η is the volume of integration of the element in the isoparametric coordinate system.

It is assumed that V is a homogeneous function of the nodal coordinates. It is also assumed that a linear displacement field can be expressed exactly in terms of the shape functions. Under these conditions, the uniform strain approach of Ref. 8 states that the nodal forces f_{iI} associated with element stresses are given by

$$f_{iI} = \sigma_{ij} B_{jI} \tag{5}$$

where σ_{ij} are components of the Cauchy stress tensor (assumed constant throughout the element), and

$$B_{jI} = \frac{\partial V}{\partial x_{jI}} \tag{6}$$

In addition, one has

$$V = x_{jI} B_{jI} \quad \text{for} \quad j = 1, 2, 3 \tag{7}$$

where there is no summation over the index j in Eq. (7).

Closed-form expressions for B_{jI} are presented in Ref. 8 for the 8-node hexahedron. Similar expressions can be derived for other element types, but they are quite lengthy for higher-order elements. As an alternative to deriving closed-form expressions for specific element types, one can use Gauss quadrature to determine B_{jI} for any isoparametric element in a systematic manner.

By substituting Eqs. (1), (3) and (4) into Eq. (6), one finds that the functions g_{jI} used by the quadrature rule to evaluate B_{jI} are given by

$$g_{1I} = \phi_{I,1}(x_{2,2}x_{3,3} - x_{3,2}x_{2,3}) + \phi_{I,2}(x_{2,3}x_{3,1} - x_{3,3}x_{2,1}) + \phi_{I,3}(x_{2,1}x_{3,2} - x_{3,1}x_{2,2}) \quad (8)$$

$$g_{2I} = \phi_{I,1}(x_{3,2}x_{1,3} - x_{1,2}x_{3,3}) + \phi_{I,2}(x_{3,3}x_{1,1} - x_{1,3}x_{3,1}) + \phi_{I,3}(x_{3,1}x_{1,2} - x_{1,1}x_{3,2}) \quad (9)$$

$$g_{3I} = \phi_{I,1}(x_{1,2}x_{2,3} - x_{2,2}x_{1,3}) + \phi_{I,2}(x_{1,3}x_{2,1} - x_{2,3}x_{1,1}) + \phi_{I,3}(x_{1,1}x_{2,2} - x_{2,1}x_{1,2}) \quad (10)$$

where

$$\phi_{I,j} = \partial\phi_I/\partial\eta_j \quad (11)$$

$$x_{i,j} = \partial x_i/\eta_j = x_{iI}(\partial\phi_I/\partial\eta_j) \quad (12)$$

and g_{jI} is evaluated at each of the quadrature points. Exact values of B_{jI} can be obtained using 2-point Gauss quadrature in three dimensions (8 quadrature points total) for the 8-node hexahedron. For the 20-node serendipity or 27-node Lagrange hexahedron, 3-point Gauss quadrature in three dimensions (27 quadrature points total) is required. Exact values of B_{jI} for the 4-node linear tetrahedron can be obtained using a 1-point quadrature rule for tetrahedral domains while the 10-node quadratic tetrahedron requires a 5-point quadrature rule. Quadrature rules for integration over tetrahedral domains are available in Ref. 5.

Following the development in Ref. 8, one can show that

$$\int_\Omega \frac{\partial \phi_I}{\partial x_j} dV = B_{jI} \tag{13}$$

where Ω is the domain of the element in the global coordinate system. Based on Eq. (13), the uniform strain ϵ^u of the element is expressed in terms of nodal displacements as

$$\epsilon^u = Cu \tag{14}$$

where

$$\epsilon^u = \left[\begin{array}{cccccc} \epsilon^u_{11} & \epsilon^u_{22} & \epsilon^u_{33} & \gamma^u_{12} & \gamma^u_{23} & \gamma^u_{31} \end{array} \right] \tag{15}$$

$$C = \frac{1}{V} \left[\begin{array}{ccccccccc} B_{11} & 0 & 0 & B_{12} & 0 & 0 & \cdots & B_{1N} & 0 & 0 \\ 0 & B_{21} & 0 & 0 & B_{22} & 0 & \cdots & 0 & B_{2N} & 0 \\ 0 & 0 & B_{31} & 0 & 0 & B_{32} & \cdots & 0 & 0 & B_{3N} \\ B_{21} & B_{11} & 0 & B_{22} & B_{12} & 0 & \cdots & B_{2N} & B_{1N} & 0 \\ 0 & B_{31} & B_{21} & 0 & B_{32} & B_{22} & \cdots & 0 & B_{3N} & B_{2N} \\ B_{31} & 0 & B_{11} & B_{32} & 0 & B_{21} & \cdots & B_{3N} & 0 & B_{1N} \end{array} \right] \tag{16}$$

and

$$u = \left[\begin{array}{cccccccccc} u_{11} & u_{21} & u_{31} & u_{12} & u_{22} & u_{32} & \cdots & u_{1N} & u_{2N} & u_{3N} \end{array} \right]^T \tag{17}$$

Elements based on the uniform strain approach have the appealing feature that they pass first-order patch tests.

Boundaries of three-dimensional elements are defined either by planar or curved faces. Elements with interpolation functions that vary linearly, e.g. the 4-node tetrahedron, have planar faces. In contrast, elements with higher-order interpolation functions, e.g. the 8-node hexahedron and 10-node tetrahedron, generally have curved faces. That being the case, it may not be obvious how to connect two meshes of elements which use different orders of interpolation along their boundaries.

Difficulties can arise using the standard master-slave approach even if the boundaries of both meshes are defined by planar faces. As was mentioned previously, even though the slave nodes stay attached to the master surface, there may not be any constraints to keep a node on the master boundary from penetrating or pulling away from the slave boundary. Such problems are addressed with the present method by requiring the faces of elements on the slave boundary to always conform to the master boundary. In order to explain how this is done, some preliminary geometric concepts are introduced first.

Notice from Eqs. (6), (14) and (16) that the relationship between strain and displacement for a uniform strain element is defined completely by its volume. Consequently, the *uniform strain* characteristics of two elements are identical if the expressions for their volumes are the same. This fact is important because it allows one to consider alternative interpolation functions for elements with faces on the master and slave surfaces. By doing so, one can interpret the present method as an approach for generating "conforming" finite elements at the shared boundary by carefully accounting for the volume (positive or negative) that exists due to an imperfect match between the two meshes both initially and during deformation.

Consider an 8-node hexahedral element whose six faces are not necessarily planar. Each point on a face of the element is associated with specific values of two isoparametric coordinates. Both the spatial coordinates and displacements of the point are linear functions of the coordinates and displacements of the four nodes defining the face. The specific forms of these relationships are obtained by setting either η_1, η_2 or η_3 equal to one of its bounding values in Eqs. (1-2).

Consider now an alternative element in which each face of the original 8-node hexahedron is triangulated with n_t facets. Each vertex of a triangular facet intersects one of the curved

faces of the hexahedron. A center node c is introduced in the interior of the element. Although the precise location of c is not important, its coordinates can be expressed in terms of those of the hexahedron as

$$x_{ic} = \sum_{I=1}^{8} x_{iI}/8 \tag{18}$$

The center node along with the three vertices of each triangular facet form the vertices of a 4-node tetrahedron. Thus, the domain of the hexahedron can be divided into $6n_t$ tetrahedral regions. Within each of these regions the interpolation functions are linear. In other words, the displacement of a point in a tetrahedral region is determined by its location and the displacements of the four nodes defining the tetrahedron. One may approximate the boundary of the original hexahedron to any level of accuracy by increasing the number of triangular facets.

Although the two elements described in the previous paragraphs are significantly different, their uniform strain characteristics are approximately the same. In the limit as n_t approaches infinity, the uniform strain characteristics of the two elements are identical. By viewing all the element faces on the master and slave surfaces as connected triangular facets, one can develop a systematic method for connecting the two meshes that passes first-order patch tests. We note that the alternative element satisfies the basic assumptions of the uniform strain approach. That is, the element volume is a homogeneous function of the nodal coordinates and a linear displacement field can be expressed exactly in terms of the interpolation functions.

We are now in a position to present the method for modifying elements with faces on the slave boundary. Changes to elements with faces on the master boundary are not required.

The concept of alternative piecewise-linear interpolation functions was introduced in the previous paragraphs to facilitate interpretation of the method as a means for generating conforming elements at the master-slave interface. These alternative interpolation functions are never used explicitly to modify the element formulations.

Figure 1 depicts the projection of an element face F_1 of the slave surface onto the master surface. The larger filled circles designate nodes on the slave surface constrained to the master surface. Smaller filled circles designate nodes on the master surface. Circles that are not filled designate the projections of slave element edges onto master element edges.

Although there are several options for projecting slave element entities onto the master surface, we opted for the following in this study. Nodes on the slave surface that are initially off the master surface are repositioned to specific points on the master surface based on a minimum distance criterion. That is, a node on the slave surface is moved and constrained to the nearest point on the master surface. For each element face of the slave surface, one can define a normal direction at the center of the face. If an element edge of the slave surface is shared by two elements, the normal direction for the edge is defined as the average of the two elements sharing the edge. Otherwise, the normal direction is chosen as that of the single element containing the edge. A plane is constructed which contains two nodes of the slave element edge and has a normal in the direction of the cross product of the element edge and the element edge normal. The projection of the slave element edge onto a master element edge is simply the intersection of this plane with the master element edge.

Let P denote the element face of the master surface onto which a node S of the slave surface is projected. The projection of S onto P can be characterized by two isoparametric coordinate values η_{1S} and η_{2S}. As a result of constraining S to P, the spatial coordinates of

S are expressed as

$$x_{iS} = x_{iK} a_{KS} \tag{19}$$

where K ranges over all the nodes defining P. The coefficient a_{KS} in Eq. (19) can be expressed in terms of η_{1S} and η_{2S} by the equation

$$a_{KS} = \phi_K^P(\eta_{1S}, \eta_{2S}) \tag{20}$$

where ϕ_K^P is the shape function of node K on face P.

The basic idea of the following development is to replace F_1 with a new boundary which prevents the possibility for overlaps or gaps between the two meshes. The new boundary is composed of two parts. The first part is denoted by F_m and consists of the projection of F_1 onto the master surface (see Figure 1). The second part is denoted by F_r and consists of ruled surfaces between the edges of F_1 and their projections onto the master surface. These two parts of the new boundary are discussed in greater detail subsequently.

Using the divergence theorem, element volume can be expressed in terms of surface integrals over the faces of the element as

$$V = \sum_{k=1}^{N_f} \int_{F_k} x_j n_j^k dS \quad \text{for} \quad j = 1, 2, 3 \tag{21}$$

where N_f is the number of element faces, F_k denotes face k, and $\mathbf{n}^k = n_j^k \mathbf{e}_j$ is the unit outward normal to F_k. Let $\hat{V}$ denote the volume of a uniform strain element obtained by replacing F_1 with the new boundary. It follows from Eq. (21) that

$$\hat{V} = V - \int_{F_1} x_j n_j^1 dS - \int_{F_m} x_j n_j^m dS + \int_{F_r} x_j n_j^r dS \quad \text{for} \quad j = 1, 2, 3 \tag{22}$$

where $\mathbf{n}^m = n_j^m \mathbf{e}_j$ is the unit outward normal to F_m and $\mathbf{n}^r = n_j^r \mathbf{e}_j$ is the unit outward normal to F_r. Notice that a negative sign is assigned to the third term on the right hand

side of Eq. (22) because $\mathbf{n}^m$ points into the slave element. The analog to Eq. (6) for the uniform strain element is given by

$$\hat{B}_{j\hat{I}} = \frac{\partial \hat{V}}{\partial x_{j\hat{I}}} \tag{23}$$

The index $\hat{I}$ is used instead of I in Eq. (23) to remind the reader that $\hat{V}$ depends on the coordinates of the original element nodes as well as the nodes defining F_m. To be specific, the index $\hat{I}$ takes on all values of I for the original element except the numbers of nodes constrained to the master boundary. In addition, $\hat{I}$ takes on the numbers of all nodes defining F_m.

Substituting Eqs. (19) and (22) into Eq. (23), one obtains

$$\begin{aligned} \hat{B}_{j\hat{I}} &= B_{j\hat{I}} + a_{\hat{I}S}\left[B_{jS} + \frac{\partial}{\partial x_{jS}}\left(\int_{F_r} x_j n_j^r dS - \int_{F_1} x_j n_j^1 dS\right)\right] \\ &\quad + \frac{\partial}{\partial x_{j\hat{I}}}\left(\int_{F_r} x_j n_j^r dS - \int_{F_m} x_j n_j^m dS\right) \quad \text{for} \quad j = 1,2,3 \end{aligned} \tag{24}$$

where the index S takes on the numbers of nodes constrained to the master boundary. Notice that $B_{j\hat{I}} = 0$ if $\hat{I}$ refers to a node on the master boundary. In addition, $a_{\hat{I}S}$ is zero if $\hat{I}$ refers to node numbers of the original element. The terms involving surface integrals on the right hand side Eq. (24) can be calculated using numerical integration as described in the following paragraphs.

The coordinates of points on F_1 can be expressed as

$$x_i = x_{iS}\phi_S(\eta_1, \eta_2) \tag{25}$$

where ϕ_S is the shape function of node S on F_1. Using Eq. (25) and a fundamental result for surface integrals, one obtains

$$\frac{\partial}{\partial x_{jS}}\int_{F_1} x_j n_j^1 dS = \int_{A_{\eta 1}} \phi_S \epsilon_{jkm} x_{k,1} x_{m,2} dA \quad \text{for} \quad j = 1,2,3 \tag{26}$$

where ϵ_{jkm} is the permutation symbol and $A_{\eta 1}$ is the area of integration for F_1 in the η_1-η_2 coordinate system. Exact values of the integral on the right hand side of Eq. (26) can be obtained using 2-point Gauss quadrature in two dimensions (4 quadrature points total) for the 8-node hexahedron. For the 20-node and 27-node hexahedron, 3-point Gauss quadrature in two dimensions (9 quadrature points total) is required. Exact values for the 4-node tetrahedron can be obtained using a 1-point quadrature rule for triangular domains while the 10-node tetrahedron requires a 7-point quadrature rule. Quadrature rules for integration over triangular domains are available in Refs. 5 and 9.

The projection of F_1 onto an element face of the master surface is shown in Figure 2. For each such master element face, the boundary of the projection is defined by a closed polygon consisting of straight-line segments in the isoparametric coordinate system of the master element face. This polygon is decomposed into triangular regions (again in the isoparametric coordinate system of the master element face) as shown to facilitate the calculation of surface integrals.

The coordinates of points on the element face can be expressed as

$$x_i = x_{iM}\phi_M(\eta_1, \eta_2) \tag{27}$$

where ϕ_M is the shape function for node M on the element face. From Eq. (27) one obtains

$$\frac{\partial}{\partial x_{jM}} \int_{F_{1f}} x_j n_j^1 dS = \int_{A_{\eta f}} \phi_M \epsilon_{jkm} x_{k,1} x_{m,2} dA \quad \text{for} \quad j = 1, 2, 3 \tag{28}$$

where F_{1f} denotes the projection of F_1 onto the element face and $A_{\eta f}$ is the area of integration of the element face in the η_1-η_2 coordinate system. The integral on the right hand side of Eq. (28) is determined by adding the contributions from each triangular region. The surface integrals can be calculated exactly for each triangular region by using the following

quadrature rules for triangular domains: 1-point for 4-node tetrahedron, 4-point for 8-node hexahedron, 7-point for 10-node tetrahedron, 13-point for 20-node hexahedron, and 19-point for 27-node hexahedron. Surface integrals in Eq. (24) over the domain F_m are obtained from Eq. (28) by summing the contributions from all involved element faces on the master surface.

Recall that the second part of the boundary to replace F_1 consists of ruled surfaces between the edges of F_1 and their projections onto the master surface. These surfaces must be considered only if the edges of F_1 do not lie entirely on the master surface. By including these surfaces, the "new boundary" of the slave element is ensured to be closed.

An edge of F_1 and its projection onto the master surface is shown in Figure 3. The spatial coordinates of points along the edge can be expressed as

$$x_{ie} = x_{iS}\phi_{Se}(\xi_2) \tag{29}$$

where ϕ_{Se} is the shape function of node S on the edge of interest.

The projection of the edge onto a participating element face of the master surface appears as one or more connected straight-line segments in the coordinate system of the element face. For each such segment, the isoparametric coordinates of points along the segment can be expressed as

$$\eta_1 = a_1 + b_1\xi_2 \tag{30}$$

$$\eta_2 = a_2 + b_2\xi_2 \tag{31}$$

where the coefficients a and b appearing in Eqs. (30-31) are determined from the projections of nodes and edges of F_1 described previously. Thus, the spatial coordinates of points along the segment can be expressed as

$$x_{ig} = x_{iM}\phi_M(a_1 + b_1\xi_2, a_2 + b_2\xi_2) \tag{32}$$

where ϕ_M is the shape function of node M on the element face.

The ruled surface between the segment and the edge is denoted by F_{ge}. Spatial coordinates of points on this surface are given by

$$x_i = (1-\xi_1)x_{ig} + \xi_1 x_{ie} \tag{33}$$

where $0 \leq \xi_1 \leq 1$. The bounding values of ξ_2 which define F_{ge} are determined from the projections described previously. It follows from Eqs. (29-33) that

$$\frac{\partial}{\partial x_{jM}} \int_{F_{ge}} x_j n_j^r dS = \int_{A_{\xi r}} \phi_M \epsilon_{jkm} \tilde{x}_{k,1} \tilde{x}_{m,2} (1-\xi_1) dA \quad \text{for} \quad j = 1,2,3 \tag{34}$$

$$\frac{\partial}{\partial x_{jS}} \int_{F_{ge}} x_j n_j^r dS = \int_{A_{\xi r}} \phi_{Se} \epsilon_{jkm} \tilde{x}_{k,1} \tilde{x}_{m,2} \xi_1 dA \quad \text{for} \quad j = 1,2,3 \tag{35}$$

where $A_{\xi r}$ is the area of integration for F_{ge} in the ξ_1-ξ_2 coordinate system, and

$$\tilde{x}_{i,1} = x_{iS}\phi_{Se} - x_{iM}\phi_M(a_1 + b_1\xi_2, a_2 + b_2\xi_2) \tag{36}$$

$$\tilde{x}_{i,2} = x_{iM}[(\partial\phi_M/\partial\eta_1)b_1 + (\partial\phi_M/\partial\eta_2)b_2](1-\xi_1) + x_{iS}(\partial\phi_{Se}/\partial\xi_2)\xi_1 \tag{37}$$

The integrals on the right hand sides of Eqs. (34-35) can be calculated exactly using a 2-point Gauss quadrature rule in the ξ_1 direction. For edges on the slave surface with three or fewer nodes, the following quadrature rules for the ξ_2 direction are sufficient: 3-point for a 4-node tetrahedron or 8-node hexahedron with a face on the master surface, 4-point for a 6-node tetrahedron or a 20-node hexahedron, and 6-point for a 27-node hexahedron. The surface integrals in Eq. (24) over the domain F_r are obtained from Eqs. (34-35) by summing the contributions from all involved segments on the master surface.

If the slave surface consists entirely of uniform strain elements, then all the necessary corrections are contained in $\hat{B}_{j\hat{I}}$. By using Eqs. (24) to calculate $\hat{B}_{j\hat{I}}$ for elements with

faces on the slave surface, one can perform analyses of connected meshes for both linear and nonlinear problems. A general method of hourglass control [10] can also be used to stabilize any elements on the boundary with spurious zero energy deformation modes.

The remainder of this section is concerned with extending the method to accommodate more commonly used finite elements on the slave surface. Although we believe the method can be extended easily to nonlinear problems, attention is restricted presently to the linear case. Needless to say, many problems of practical interest are in this category.

Prior to any modifications, the stiffness matrix K of an element with a face on the slave surface can be expressed as

$$K = K_u + K_r \tag{38}$$

where K_u denotes the uniform strain portion of K and K_r is the remainder. The matrix K_u is defined as

$$K_u = VC^T DC \tag{39}$$

where D is a material matrix that is assumed constant throughout the element. Recall that V is the element volume and C is given by Eq. (16). Substituting Eq. (39) into Eq. (38) and solving for K_r yields

$$K_r = K - VC^T DC \tag{40}$$

Let u^l denote the vector u (see Eq. 17) obtained by sampling a linear displacement field at the nodes. The nodal forces f^l associated with u^l are given by

$$f^l = Ku^l \tag{41}$$

For a properly formulated element, one has

$$K_u u^l = f^l \tag{42}$$

and

$$K_r u^l = 0 \tag{43}$$

If Eq. (42) does not hold, then $K_u u^l \neq f^l$ and elements based on the uniform strain approach would fail a first-order patch test. Equation (43) implies that K_r does not contribute to the nodal forces for linear displacement fields.

The basic idea of the following development is to alter the uniform strain portion of the stiffness matrix while leaving K_r unchanged. Let $\hat{u}$ denote the displacement vector for nodes associated with the index $\hat{I}$ (see discussion following Eq. 23). Based on the constraints in Eq. (19), one may express u in terms of $\hat{u}$ as

$$u = G\hat{u} \tag{44}$$

where G is a transformation matrix. The modified stiffness matrix $\hat{K}$ of the element is defined as

$$\hat{K} = \hat{V}\hat{C}^T D\hat{C} + G^T K_r G \tag{45}$$

where $\hat{C}$ denotes the matrix C (see Eq. 16) associated with $\hat{B}_{j\hat{I}}$ (see Eq. 24). The stiffness matrix K_{ms} obtained using the standard master-slave approach is given by

$$K_{ms} = G^T K G \tag{46}$$

Comparing $\hat{K}$ with K_{ms}, one finds that

$$\hat{K} - K_{ms} = \hat{V}\hat{C}^T D\hat{C} - G^T(VC^T DC)G \tag{47}$$

The right hand side of Eq. (47) is simply the difference between the uniform strain portions of $\hat{K}$ and K_{ms}. If continuity at the master-slave interface holds by satisfying Eq. (44)

alone, then the surfaces integrals in Eq. (24) sum to zero and $\hat{K} = K_{ms}$. Thus, under such conditions, the present method and the standard master-slave approach are equivalent.

Prior to element modifications, the strain ϵ in an element on the slave surface can be expressed as

$$\epsilon = Cu + Hu \tag{48}$$

where Cu is the uniform strain (see Eq. 14) and Hu is the remainder. The modified element strain $\hat{\epsilon}$ is defined as

$$\hat{\epsilon} = \hat{C}\hat{u} + Hu \tag{49}$$

Equation (49) is used to calculate the strains in elements with faces on the slave surface.

One might erroneously consider developing a modified stiffness matrix $\hat{K}_{\hat{\epsilon}}$ based on Eq. (49). The result is

$$\hat{K}_{\hat{\epsilon}} = \hat{V}\hat{C}^T D\hat{C} + \int_{\hat{\Omega}} \left[\hat{C}^T DHG + G^T H^T D\hat{C} + G^T H^T DHG\right] dV \tag{50}$$

where $\hat{\Omega}$ denotes the domain of the element with face F_1 replaced by the new boundary. The difficulties with using $\hat{K}_{\hat{\epsilon}}$ for an element formulation are twofold. First, it may not be simple to evaluate the integral in Eq. (50) because the domain $\hat{\Omega}$ could be irregular. Second, and more importantly, such an element formulation does not pass the patch test. To explain this fact, let $\hat{u}^l$ denote the vector $\hat{u}$ obtained by sampling a linear displacement field. In general, one has $\hat{K}\hat{u}^l \neq \hat{K}_{\hat{\epsilon}}\hat{u}^l$ since the product $\hat{C}\hat{u}^l$ is not necessarily zero.

In summary, the present method alters the formulations of elements on the slave surface by accounting correctly for the volume between the two meshes that is present either initially or during deformation. A method that does not require changes to element formulations for elements on the master or slave surfaces may be preferable in certain instances. We

are currently investigating such a method based on constraint equations and the volume accounting principles explored in this study.

3. Example Problems

All the example problems in this section assume small deformations of a linear, elastic, isotropic material with Young's modulus $E = 10^7$ and Poisson's ratio $\nu = 0.3$. In this case, the material matrix D can be expressed as

$$D = \begin{bmatrix} 2G+\lambda & \lambda & \lambda & 0 & 0 & 0 \\ \lambda & 2G+\lambda & \lambda & 0 & 0 & 0 \\ \lambda & \lambda & 2G+\lambda & 0 & 0 & 0 \\ 0 & 0 & 0 & G & 0 & 0 \\ 0 & 0 & 0 & 0 & G & 0 \\ 0 & 0 & 0 & 0 & 0 & G \end{bmatrix} \tag{51}$$

where

$$G = \frac{E}{2(1+\nu)} \tag{52}$$

and

$$\lambda = \frac{E\nu}{(1+\nu)(1-2\nu)} \tag{53}$$

Five different element types are considered in the example problems. These include the 4-node tetrahedron ($T4$), eight-node hexahedron ($H8$), ten-node tetrahedron ($T10$), 20-node hexahedron ($H20$), and 27-node hexahedron ($H27$). Stiffness matrices of the various elements are calculated using numerical integration. The following quadrature rules in three dimensions are used for the hexahedral elements: 2-point for 8-node hexahedron, 3-point for 20-node hexahedron, and 3-point for 27-node hexahedron. Single-point and 5-point quadrature rules for tetrahedral domains are used for element types $T4$ and $T10$, respectively.

Two meshes connected at a shared boundary are used in all the example problems. Mesh 1 is initially bounded by the the six sides $x_1 = 0$, $x_1 = h_1$, $x_2 = 0$, $x_2 = h_2$, $x_3 = 0$

and $x_3 = h_3$ while Mesh 2 is initially bounded by $x_1 = h_1$, $x_1 = 2h_1$, $x_2 = 0$, $x_2 = h_2$, $x_3 = 0$ and $x_3 = h_3$ (see Figure 4). Each mesh consists of one of the element types described in the previous paragraph. The number of element edges in direction i for mesh m is designated by n_{im}. Thus, all the meshes in Figure 4 have $n_{11} = n_{21} = n_{31} = 2$ and $n_{12} = n_{22} = n_{32} = 3$. Specific mesh configurations are designated by the element type for Mesh 1 followed by the element type for Mesh 2.

Calculated values of the energy norm of the error are presented for purposes of comparison and for the investigation of convergence rates. The energy norm of the error is a measure of the accuracy of a finite element approximation and is defined as

$$e = \left[\sum_{k \in \mathcal{I}} \int_{\Omega_k} (\epsilon^{fe} - \epsilon^{exact})^T D (\epsilon^{fe} - \epsilon^{exact}) dV \right]^{1/2} \tag{54}$$

where Ω_k is the domain of element k and ϵ^{fe} and ϵ^{exact} denote the finite element and exact strains, respectively. The symbol $\mathcal{I}$ denotes the set of all element numbers for the two meshes. Calculation of energy norms for hexahedral and tetrahedral elements is based on the quadrature rules for element types $H20$ and $T10$, respectively.

Example 3.1

The first example is concerned with a uniaxial tension patch test and highlights some of the differences between the standard master-slave approach and the present method. The boundary conditions for the problem are given by

$$u_1(0, x_2, x_3) = 0 \tag{55}$$

$$u_2(0, 0, 0) = 0 \tag{56}$$

$$u_3(0, 0, 0) = 0 \tag{57}$$

$$u_3(0, h_2, 0) = 0 \tag{58}$$

and

$$\sigma_{11}(2h_1, x_2, x_3) = 1 \tag{59}$$

The exact solution for the displacement is given by

$$u_1(x_1, x_2, x_3) = x_1/E \tag{60}$$

$$u_2(x_1, x_2, x_3) = -\nu x_2/E \tag{61}$$

$$u_3(x_1, x_2, x_3) = -\nu x_3/E \tag{62}$$

The exact solution for stresses has all components equal to zero except for σ_{11} which equals unity. All the meshes used in the example have $h_1 = 5$, $h_2 = 10$, $h_3 = 10$, $n_{11} = n_{21} = n_{31} = n$ and $n_{12} = n_{22} = n_{32} = 3n/2$ where n is a positive even integer.

Several analyses with $n = 2$ were performed to evaluate the method. Using all five element types for Mesh 1 and Mesh 2 resulted in 25 different mesh configurations. Nodes internal to the meshes and along the master-slave interface were moved randomly so that all the elements were initially distorted. Following the initial movement of nodes, nodes on the slave boundary were repositioned to lie on the master boundary. It is noted that gaps and overlaps still remained between the two meshes after repositioning the slave surface nodes (see Figure 5). The two meshes were alternately designated as master and slave. In all cases the patch test was passed. That is, the calculated element stresses and nodal displacements were in agreement with the exact solution to machine precision.

The remaining discussion for this example deals with results obtained using the standard master-slave approach with Mesh 1 designated as master. The minimum and maximum values of σ_{11} at centroids of elements with faces on the slave surface are shown in Table 1 for

mesh configurations $H8H8$, $H20H20$, $T4T4$ and $T10T10$ for a variety of mesh resolutions. It is clear from the table that refinement of the meshes does not improve the accuracy of the solution at the shared boundary. In addition, the errors in stress at the interface are greater for mesh configuration $H20H20$ than for $H8H8$. Figure 6 shows the values of σ_{11} for mesh configuration $H8H8$ with $n = 4$. The same information is shown in Figure 7 for mesh configuration $H20H20$.

Plots of the energy norm of the error for mesh configurations $H8H8$ and $H20H20$ are shown in Figure 8. It is clear that the energy norms decrease with mesh refinement, but the convergence rates are significantly lower than those expected for elements in a single unconnected mesh. The slopes of lines connecting the first two data points are approximately 0.51 and 0.50 for $H8H8$ and $H20H20$, respectively. In contrast, the energy norms of the error for a single mesh of $H8$ or undistorted $H20$ elements have slopes which asymptotically approach 1 and 2, respectively, in the absence of singularities. The fact that displacement continuity is not satisfied at the shared boundary severely degrades the convergence characteristics of the connected meshes.

We note that the results presented in Table 1 and Figures 6-8 are for the "best case" scenario of connecting two regular meshes that conform initially. In general, two dissimilar meshes will not conform initially at all locations if the shared boundary is curved. Use of the standard master-slave approach in such cases may result in even greater errors.

Example 3.2

The second example investigates convergence rates for the present method. The specific problem considered is pure bending. The problem description is identical to Example 3.1

with the exception that the boundary condition at $x_1 = 2h_1$ is replaced by

$$\sigma_{11}(2h_1, x_2, x_3) = h_2/2 - x_2 \tag{63}$$

The exact solution has all of the stress components equal to zero except for σ_{11} which is given by

$$\sigma_{11}(x_1, x_2, x_3) = h_2/2 - x_2 \tag{64}$$

In all cases Mesh 1 was designated as master.

Plots of the energy norm of the error are shown in Figure 9 for mesh configurations $H8H8$ and $H20H20$. The slopes of lines connecting the first two data points are approximately 1.00 and 1.76 for $H8H8$ and $H20H20$, respectively. Notice that a convergence rate of unity is achieved by mesh configuration $H8H8$. Although the slopes of line segments are greater for mesh configuration $H20H20$, the optimal slope of 2 is not achieved. One should not expect to obtain a convergence rate of 2 with the present method since corrections are made only to satisfy first-order patch tests. Nevertheless, the results for mesh configuration $H20H20$ are more accurate than those for $H8H8$. Although the asymptotic rate of convergence for $H20H20$ is not clear from the figure, it is bounded below by unity.

Example 3.3

The final example demonstrates the freedom to designate master and slave boundaries independently of the resolutions of the two meshes. We consider again a problem of pure bending for mesh configuration $H8H8$ with Mesh 1 designated as master. The boundary conditions are given by

$$u_2(x_1, 0, x_3) = 0 \tag{65}$$

$$u_3(0,0,0) = 0 \tag{66}$$

$$u_1(0,0,0) = 0 \tag{67}$$

$$u_1(0,0,h_3) = 0 \tag{68}$$

and

$$\sigma_{22}(x_1,h_2,x_3) = h_1 - x_1 \tag{69}$$

The exact solution has all of the stress components equal to zero except for σ_{22} which is given by

$$\sigma_{22}(x_1,x_2,x_3) = h_1 - x_1 \tag{70}$$

All the meshes used in the example have $h_1 = 1$, $h_2 = 10$, $h_3 = 1$, $n_{11} = n_{12} = n$ and $n_{31} = n_{32} = n$. Two different cases are considered for the mesh resolutions in the 2-direction. For Case 1, $n_{21} = 5n$ and $n_{22} = 10n$. For Case 2, $n_{21} = 10n$ and $n_{22} = 5n$. Thus, for Case 1 the mesh resolution in the 2-direction of the slave surface is twice that of the master surface. In contrast, the mesh resolution in the 2-direction of the master surface is twice that of the slave surface for Case 2. Mesh resolutions in the 1 and 3 directions for Meshes 1 and 2 are the same for both cases. Results for Case 1 are identical to those obtained using the standard master-slave approach since the meshes are conforming in this case.

Plots of the energy norm of the error are shown in Figure 10 for Case 1 and Case 2. Notice that Case 2 is consistently more accurate for all the mesh resolutions considered. In order to investigate the cause of these differences, the shear stress component σ_{12} was calculated at the centroids of elements with faces on the slave surface. Results of these calculations are presented in Figures 11 and 12 for $n = 2$. The exact value of σ_{12} for this example is zero over the entire domain of both meshes. Notice that the magnitudes of σ_{12} are significantly

smaller for Case 2 than Case 1. It is thought that results for Case 2 are more accurate than those for Case 1 because fewer degrees of freedom are constrained at the shared boundary. This example shows that there may be a preferred choice for the master boundary in certain instances.

4. Conclusions

A systematic and straightforward method is presented for connecting dissimilar finite element meshes in three dimensions. By modifying the boundaries of elements with faces on the slave surface, corrections can be made to element formulations such that first-order patch tests are passed. The method can be used to connect meshes with different element types. In addition, master and slave surfaces can be designated independently of the resolutions of the two meshes.

A simple uniaxial stress example demonstrated several of the advantages of the present method over the standard master-slave approach. Although the energy norm of the error decreased with mesh refinement for the master-slave approach, the convergence rates were significantly lower than those for elements in a single unconnected mesh. Calculated stresses in elements with faces on the shared boundary had errors up to 13 and 24 percent for connected meshes of 8-node and 20-node hexahedral elements, respectively. For 4-node and 10-node tetrahedral elements, the errors were in excess of 21 percent. Moreover, these errors could not be reduced with mesh refinement.

A convergence rate of unity for the energy norm of the error was achieved for a pure bending example using connected meshes of 8-node hexahedral elements. This convergence rate is consistent with that of a single mesh of 8-node hexahedral elements. More accurate

results were obtained for connected meshes of 20-node hexahedral elements, but a convergence rate of two was not achieved. The optimal convergence rate of two was not achieved in this case because element corrections are made only to satisfy first-order patch tests.

The final example showed that improved accuracy can be achieved in certain instances by allowing the master surface to have a greater number of nodes than the slave surface. Standard practice commonly requires the master surface to have fewer numbers of nodes. By relaxing this constraint, improved results were obtained as measured by the energy norm of the error and stresses along the shared boundary.

References

1. K. K. Ang and S. Valliappan, 'Mesh Grading Technique using Modified Isoparametric Shape Functions and its Application to Wave Propagation Problems,' *International Journal for Numerical Methods in Engineering*, **23**, 331-348, (1986).

2. L. Quiroz and P. Beckers, 'Non-Conforming Mesh Gluing in the Finite Element Method,' *International Journal for Numerical Methods in Engineering*, **38**, 2165-2184 (1995).

3. D. Rixen, C. Farhat and M. Géradin, 'A Two-Step, Two-Field Hybrid Method for the Static and Dynamic Analysis of Substructure Problems with Conforming and Non-conforming Interfaces,' *Computer Methods in Applied Mechanics and Engineering*, **154**, 229-264 (1998).

4. T. Y. Chang, A. F. Saleeb and S. C. Shyu, 'Finite Element Solutions of Two-Dimensional Contact Problems Based on a Consistent Mixed Formulation,' *Computers and Structures*, **27**, 455-466 (1987).

5. O. C. Zienkiewicz and R. L. Taylor, *The Finite Element Method*, Vol. 1, 4th Ed., McGraw-Hill, New York, New York, 1989.

6. C. R. Dohrmann, S. W. Key and M. W. Heinstein, 'A Method for Connecting Dissimilar Finite Element Meshes in Two Dimensions', submitted to *International Journal for Numerical Methods in Engineering.*

7. C. R. Dohrmann and S. W. Key, 'A Transition Element for Uniform Strain Hexahedral and Tetrahedral Finite Elements,' to appear in *International Journal for Numerical Methods in Engineering.*

8. D. P. Flanagan and T. Belytschko, 'A Uniform Strain Hexahedron and Quadrilateral with Orthogonal Hourglass Control', *International Journal for Numerical Methods in Engineering*, **17**, 679-706 (1981).

9. M. E. Laursen and M. Gellert, 'Some Criteria for Numerically Integrated Matrices and Quadrature Formulas for Triangles,' *International Journal for Numerical Methods in Engineering*, **12**, 67-76 (1978).

10. C. R. Dohrmann, S. W. Key, M. W. Heinstein and J. Jung, 'A Least Squares Approach for Uniform Strain Triangular and Tetrahedral Finite Elements', *International Journal for Numerical Methods in Engineering*, **42**, 1181-1197 (1998).

Table 1: Minimum and maximum values of σ_{11} at centroids of elements with faces on the slave surface for Example 3.1. The results presented were obtained using the standard master-slave approach for different resolutions of mesh configurations $H8H8$, $H20H20$, $T4T4$ and $T10T10$. The exact value of σ_{11} is unity.

n	$H8H8$		$H20H20$		$T4T4$		$T10T10$	
	min	max	min	max	min	max	min	max
2	0.9406	1.1196	0.7697	1.1009	0.7872	1.1350	0.7898	1.1082
4	0.9313	1.1298	0.7644	1.1064	0.7689	1.1649	0.7858	1.1209
6	0.9305	1.1294	0.7642	1.1061	0.7651	1.1687	0.7854	1.1208
8	0.9304	1.1292	0.7642	1.1061	0.7639	1.1694	-	-

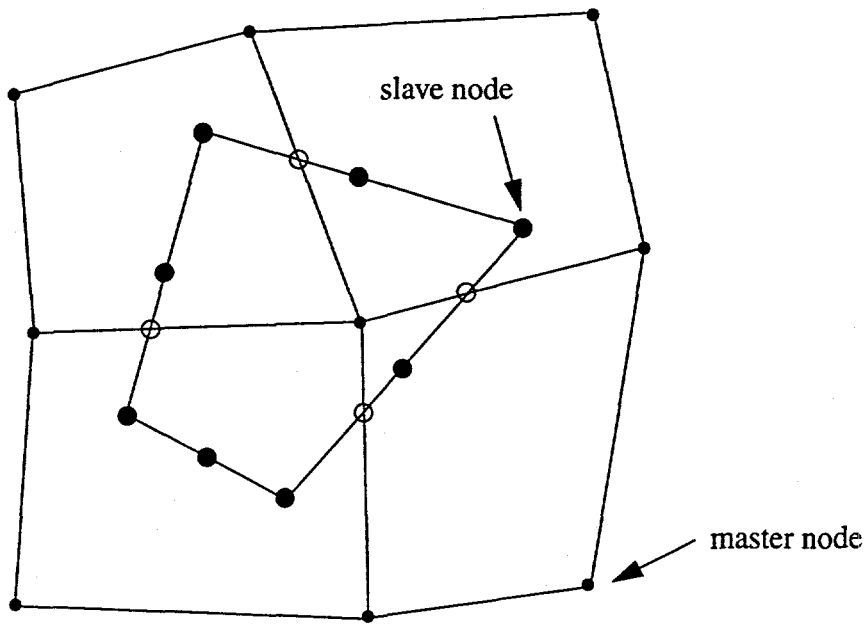

Figure 1: Projection of an element face F_1 of the slave surface onto the master surface. Larger filled circles designate nodes on the slave surface constrained to the master surface. Smaller filled circles designate nodes on the master surface. Circles that are not filled designate the projections of slave element edges onto master element edges.

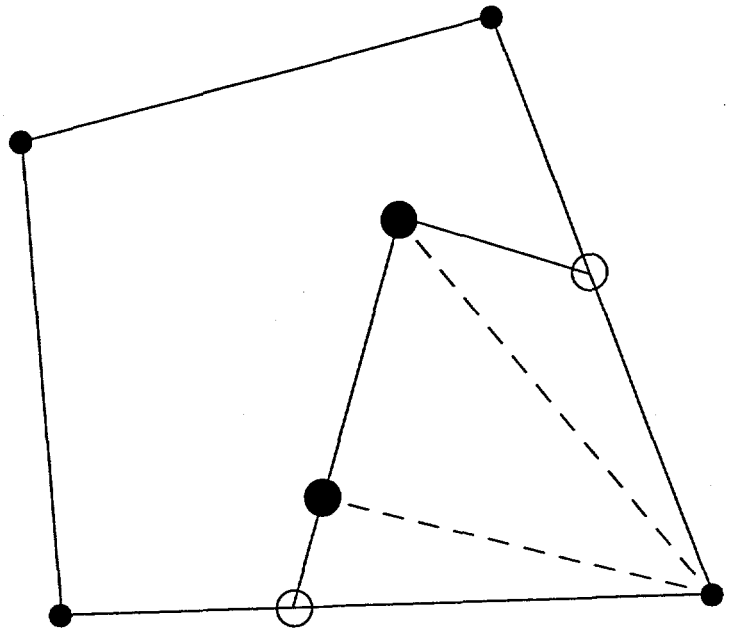

Figure 2: Projection of F_1 onto an element face of the master surface (see top left corner of Figure 1). In the coordinate system of the element face, the triangular regions have straight edges and lie in a single plane. The domain of the projection of F_1 onto the element face is divided into triangular regions for the purpose of calculating surface integrals over F_m.

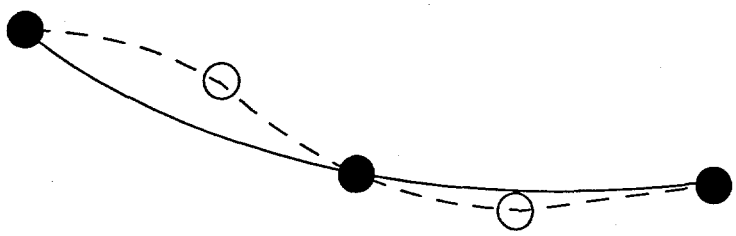

Figure 3: An edge of F_1 (solid line) and its projection onto the master surface (dashed line) viewed from a direction nearly orthogonal to F_1. The edge shown spans three different element faces on the master surface. The projection of the edge onto the master surface is a piecewise continuous line with possible discontinuities in slope at edges on the master surface. The solid and dashed lines appear as straight lines in the coordinate systems of element faces on the slave and master surfaces, respectively.

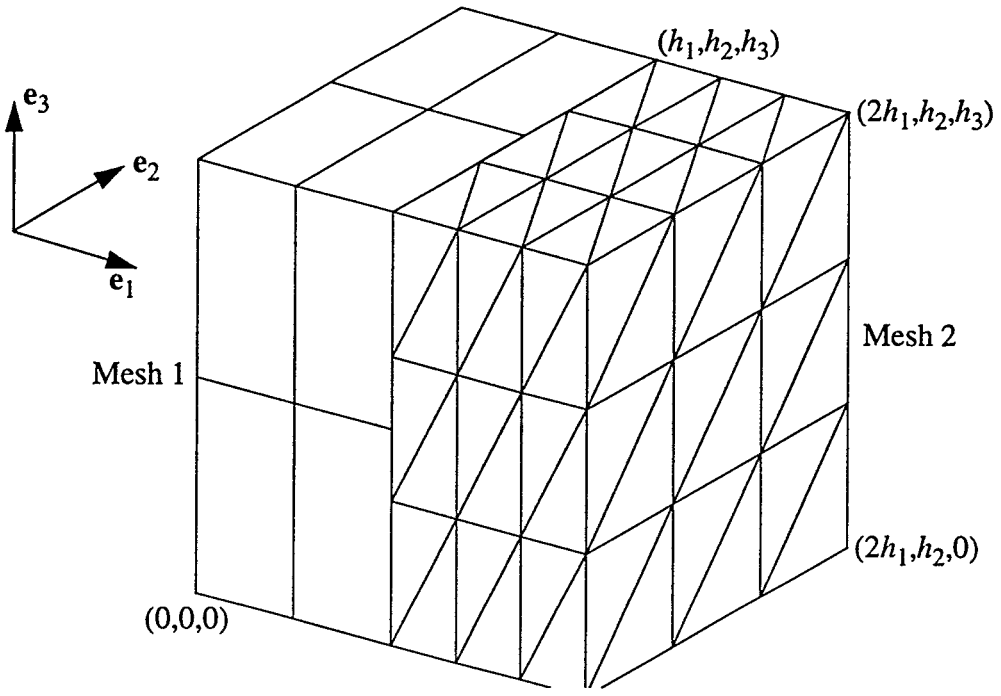

(a)

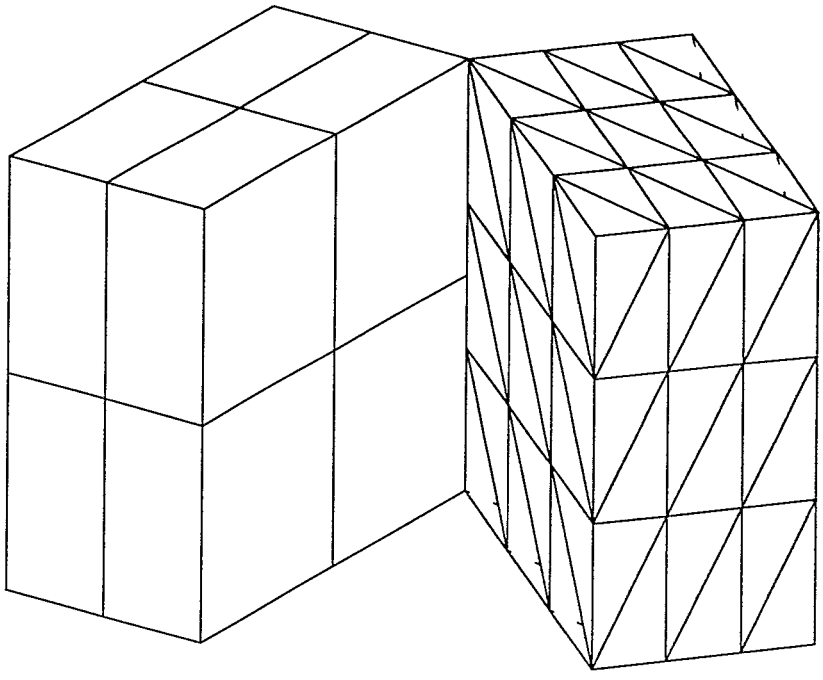

(b)

Figure 4: (a) Mesh configuration *H8T4* with $n_{11} = n_{21} = n_{31} = 2$ and $n_{12} = n_{22} = n_{32} = 3$, (b) opened view of meshes revealing shared boundary.

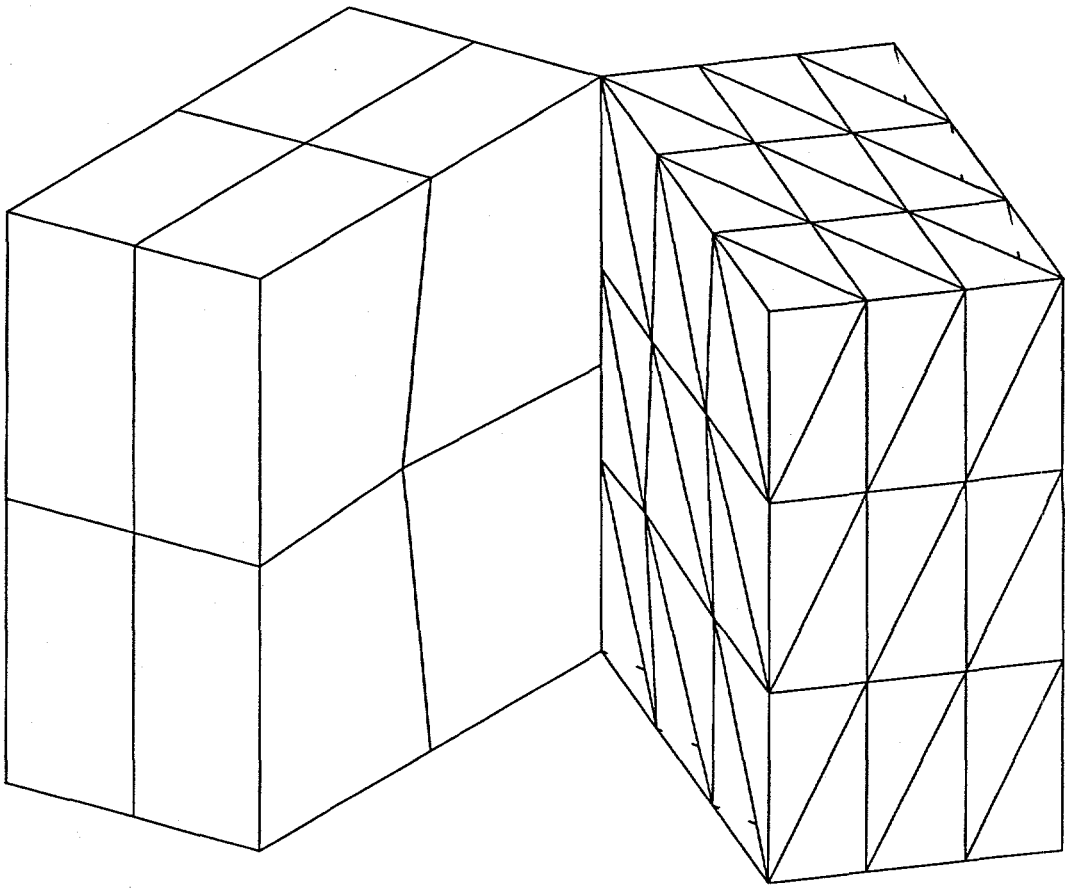

Figure 5: Opened view of mesh configuration *H8T4* with distorted elements. Although the slave nodes are repositioned to lie on the master surface, gaps and overlaps still remain between the two meshes because of the distorted element faces. Patch tests for this mesh configuration and others were passed in all cases using the present method.

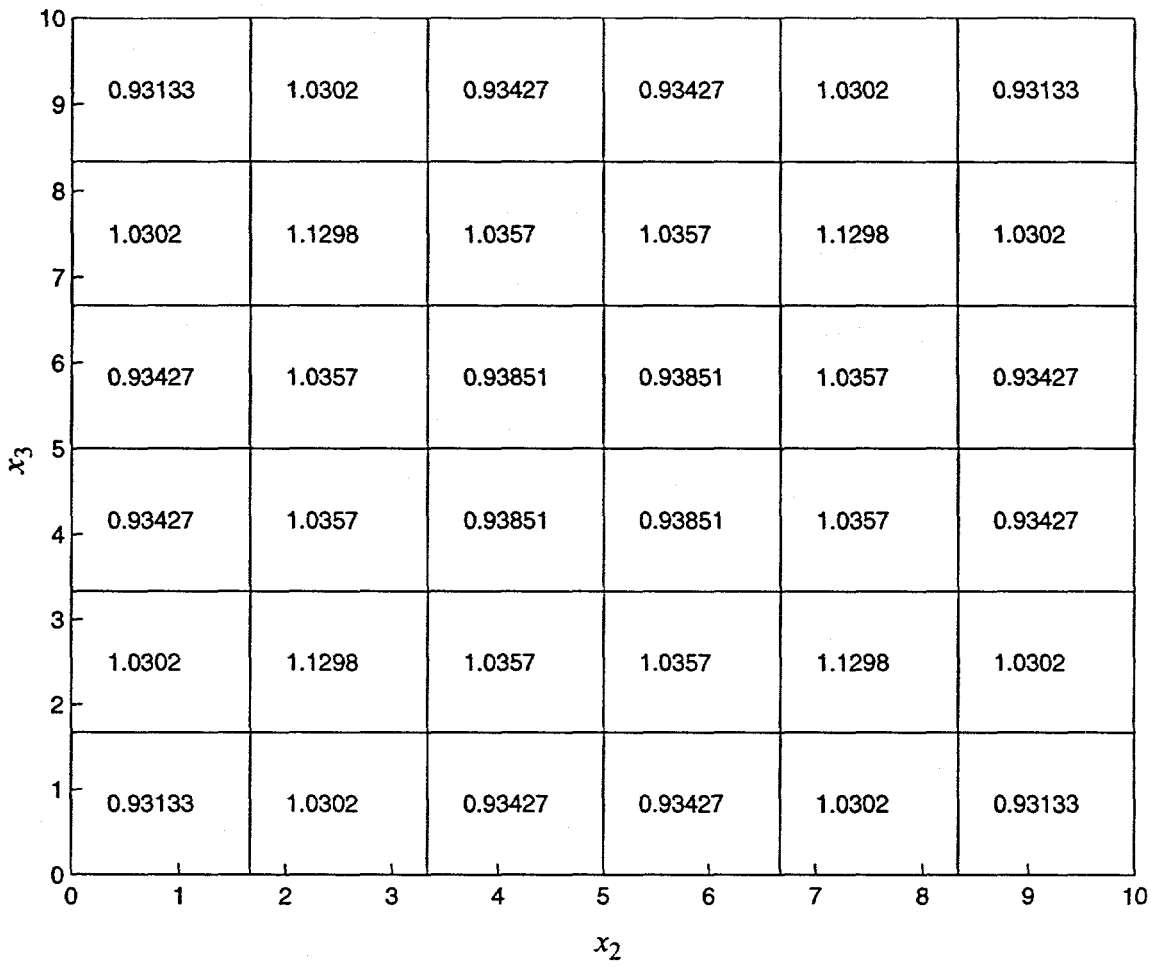

Figure 6: Stress component σ_{11} at centroids of elements with faces on the slave surface for Example 3.1. Results presented are for mesh configuration $H8H8$ using the standard master-slave approach.

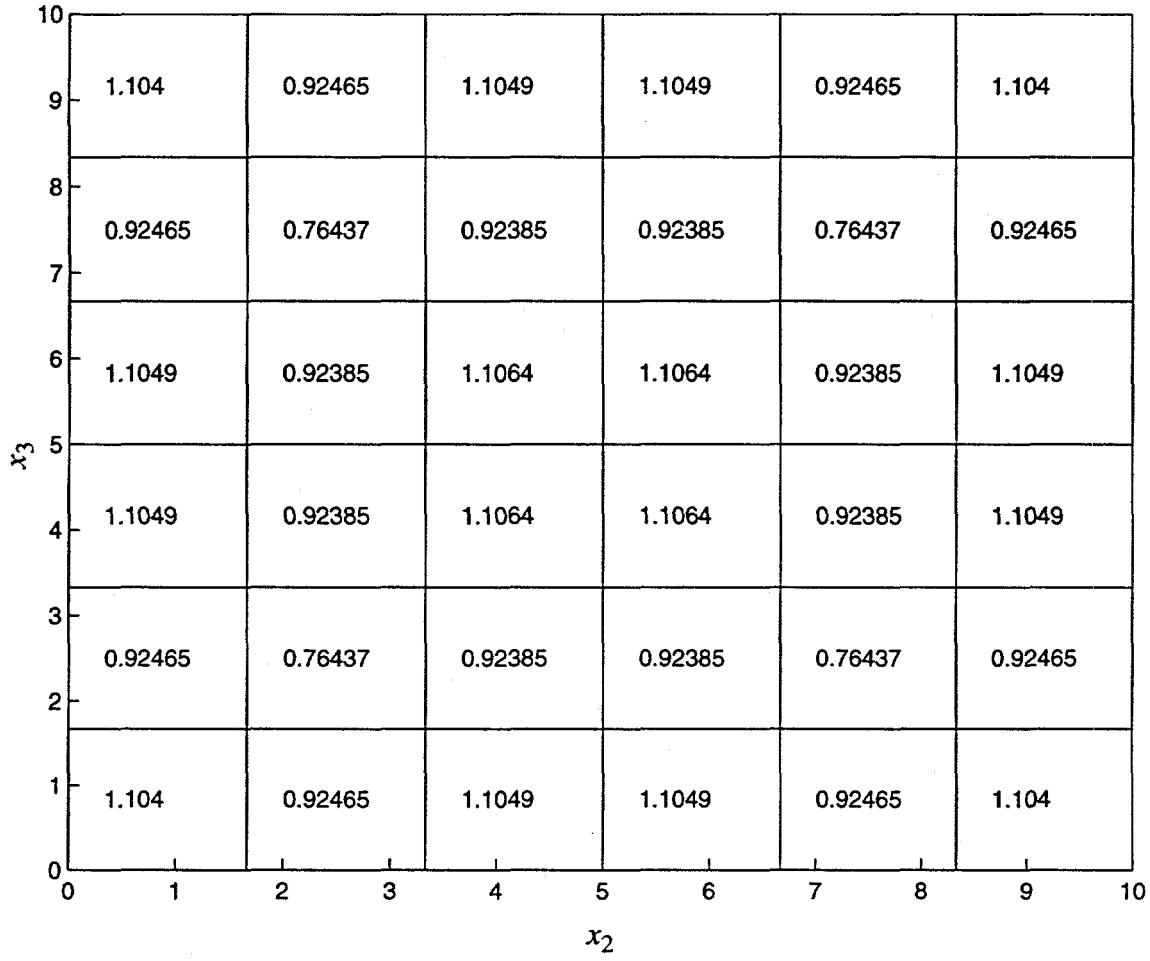

Figure 7: Stress component σ_{11} at centroids of elements with faces on the slave surface for Example 3.1. Results presented are for mesh configuration $H20H20$ using the standard master-slave approach.

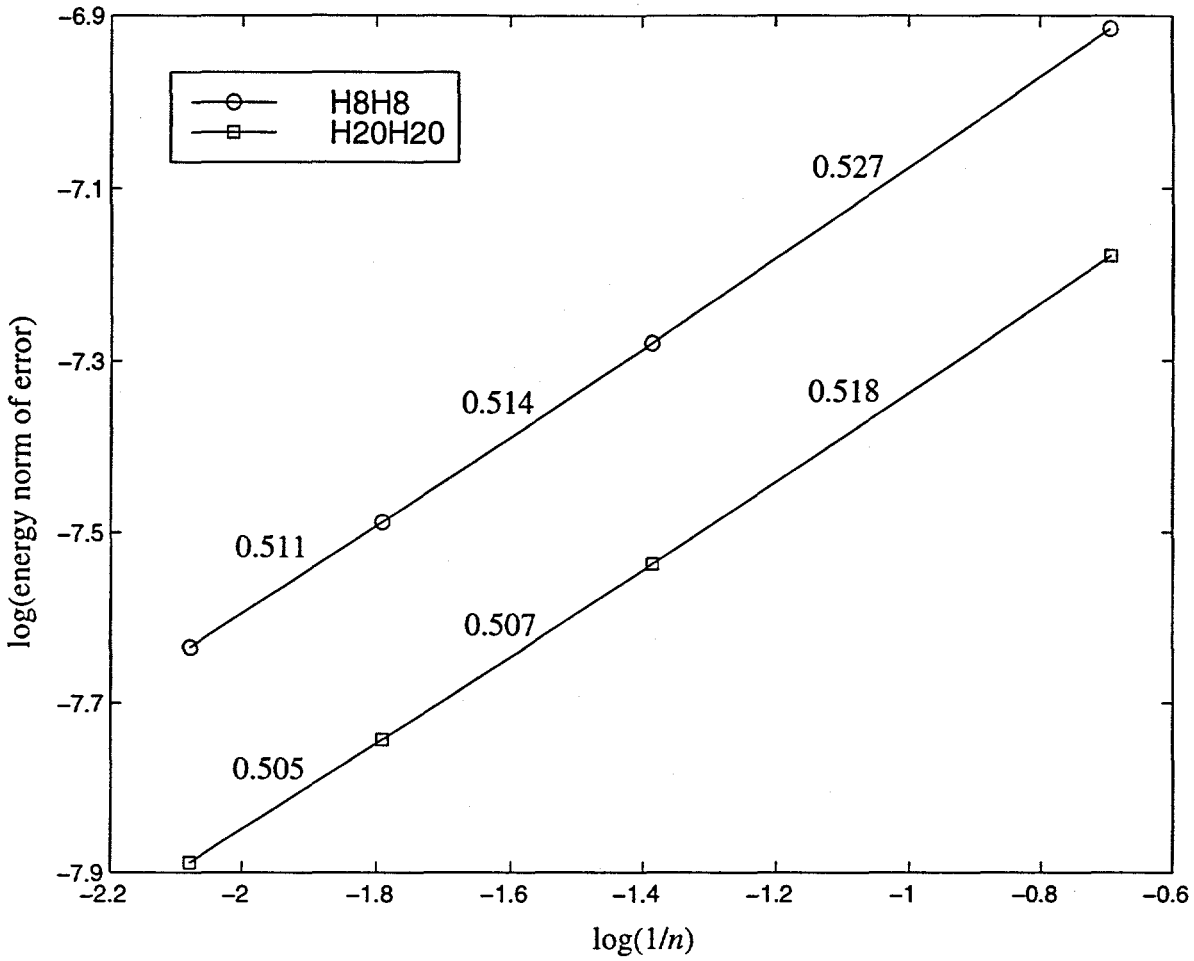

Figure 8: Energy norms of the error for Example 3.1 obtained using the standard master-slave approach. Slopes of lines connecting the data points are shown above the line segments.

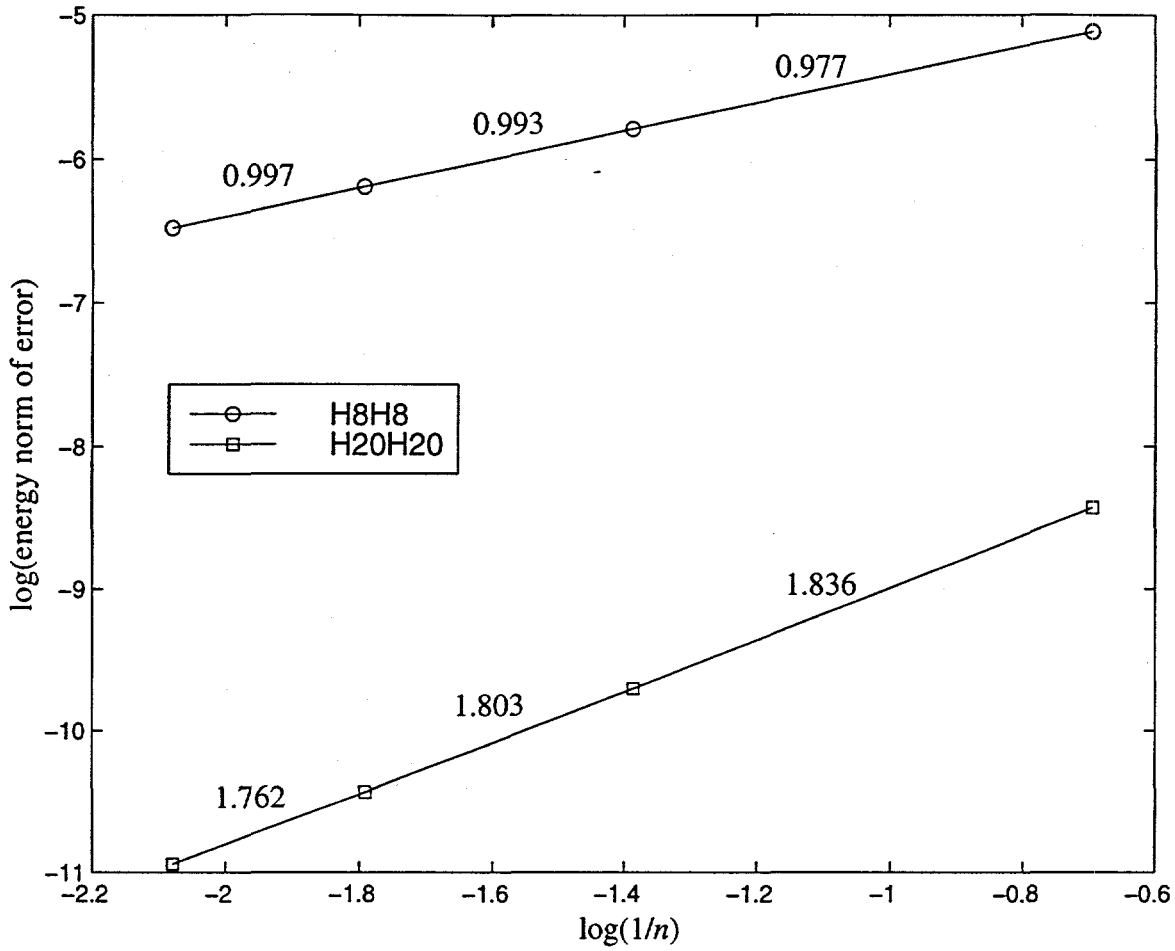

Figure 9: Energy norms of the error for Example 3.2 obtained using the present method. Slopes of lines connecting the data points are shown above the line segments.

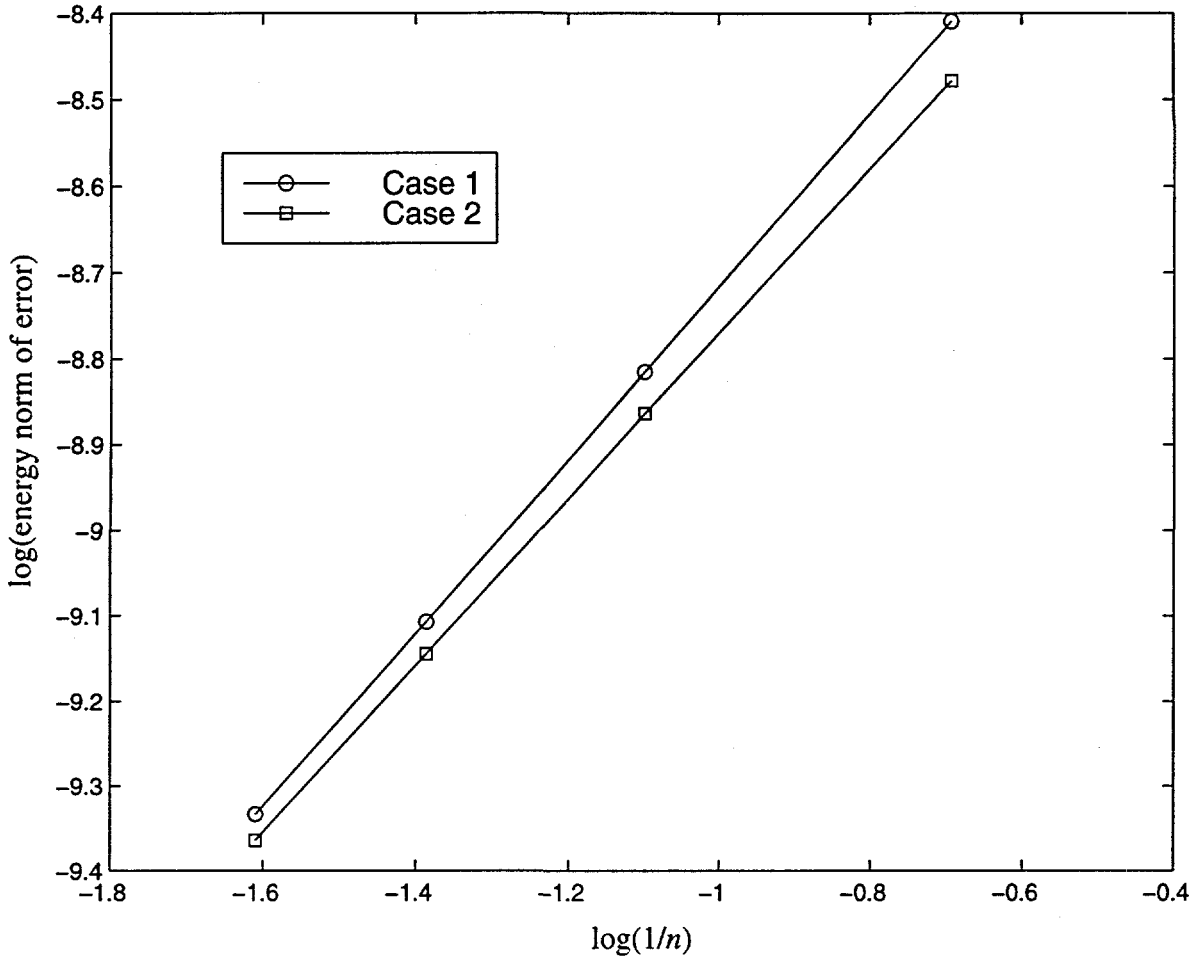

Figure 10: Energy norms of the error for Example 3.3 obtained using the present method.

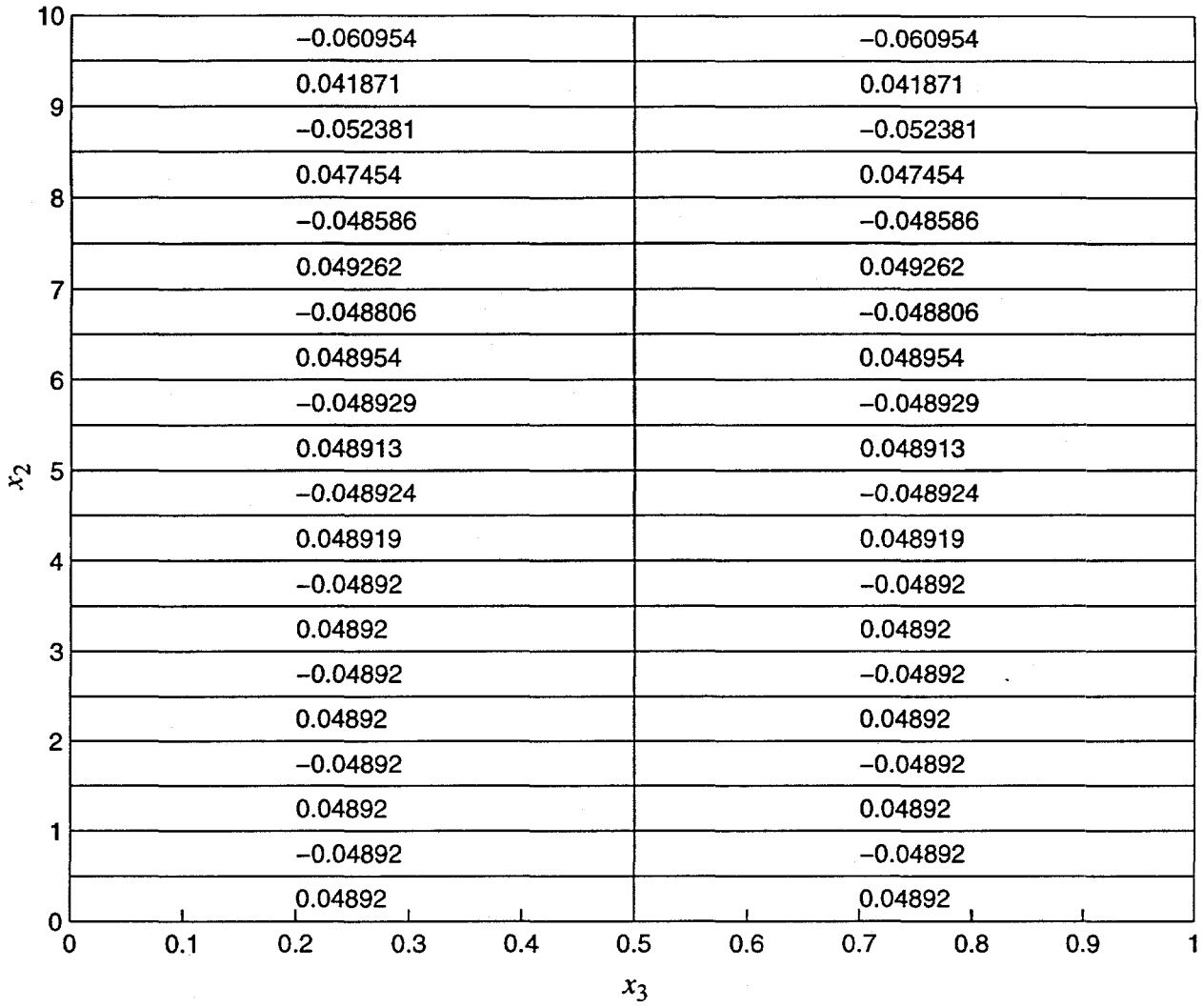

Figure 11: Stress component σ_{12} at centroids of elements with faces on the slave surface for Case 1 of Example 3.3.

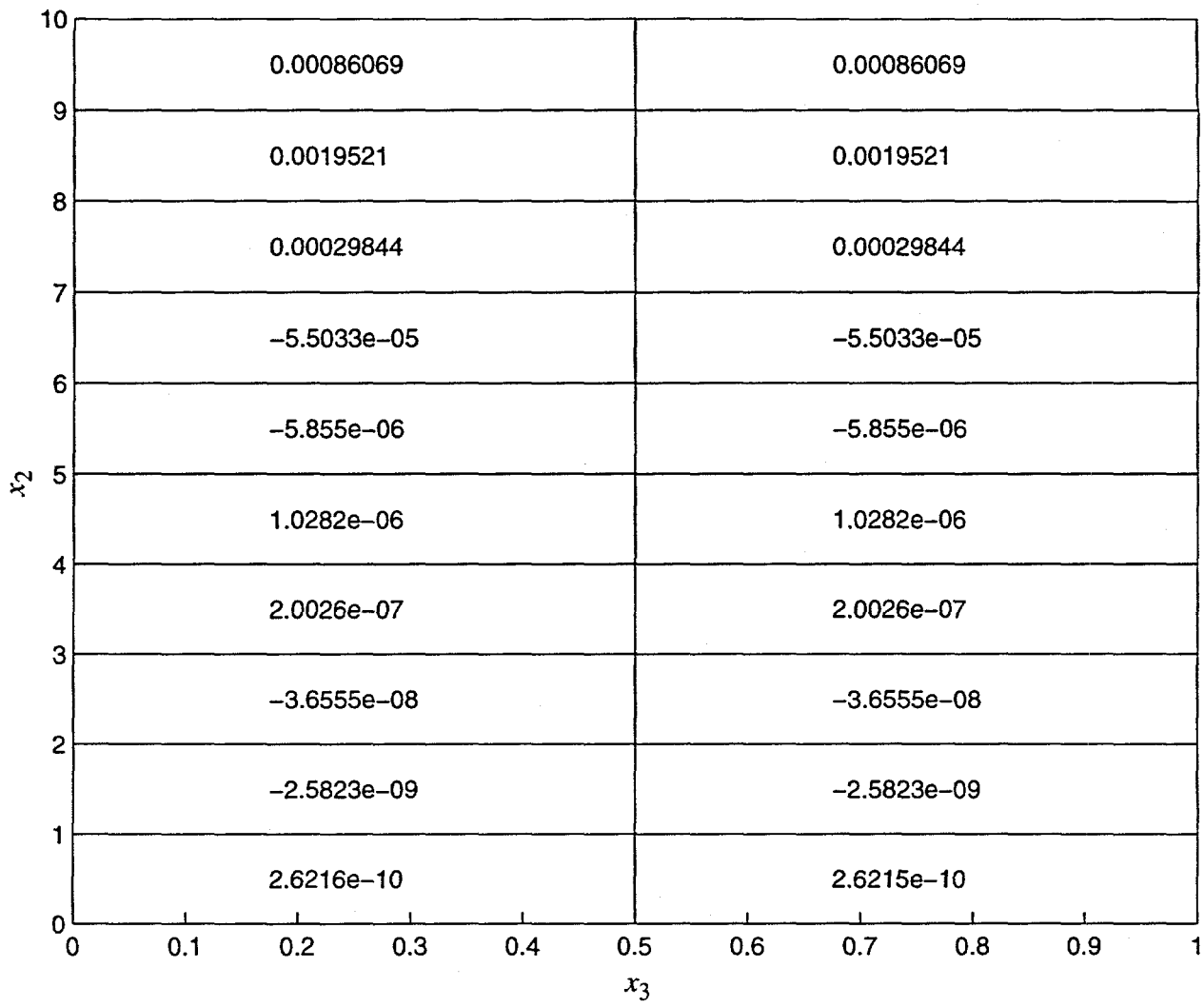

Figure 12: Stress component σ_{12} at centroids of elements with faces on the slave surface for Case 2 of Example 3.3.